

S2Vec: Self-Supervised Geospatial Embeddings

Shushman Choudhury, Elad Aharoni, Chandrakumari Suvarna, Ivel Tsogsuren, Abdul Rahman Kreidieh, Chun-Ta Lu, Neha Arora
 Google Research
 Mountain View, USA

{shushmac, eaharoni, chandrasuvarna, iveel, aboudy, chunta, nehaarora}@google.com

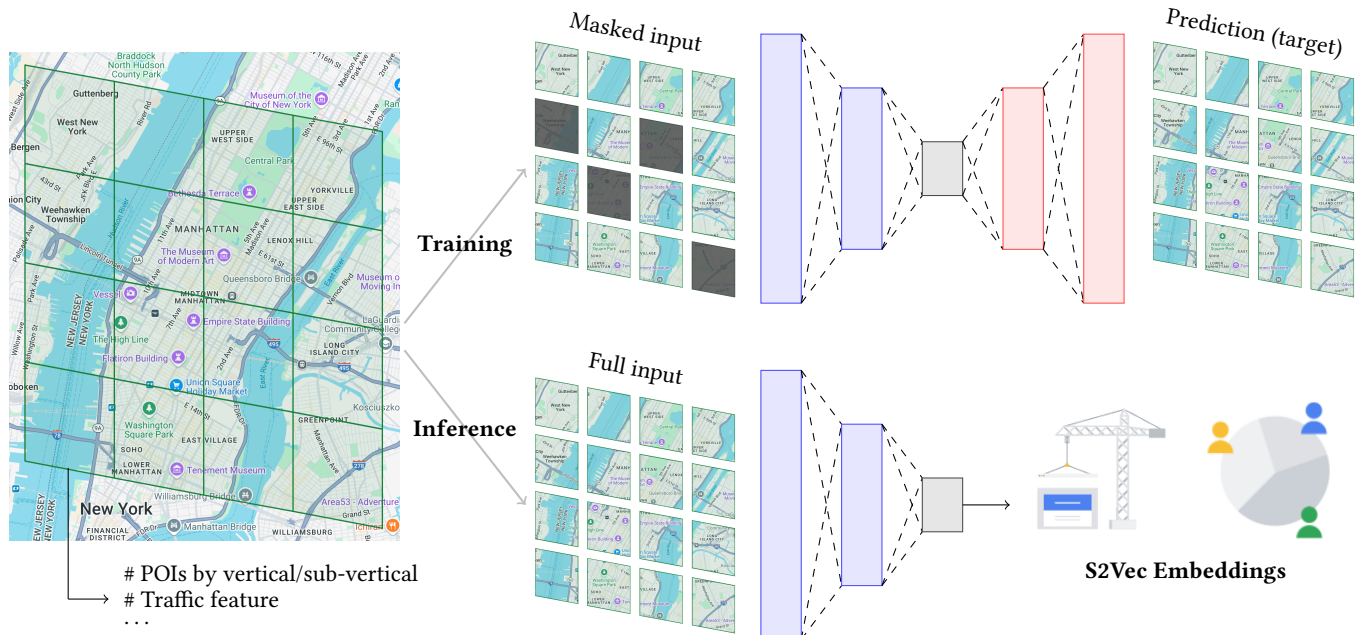


Figure 1: An overview of the S2Vec framework for learning geospatial embeddings of built environment features. We divide a large geographic area into fine-grained cells using the S2 library and construct a feature vector of built environment attributes for each fine-grained cell. We then rasterize the feature vectors as patches in an image of a larger cell, and create a dataset of such images. Finally, we run masked autoencoding, a self-supervised learning approach on this image dataset to generate embeddings for the patches. The S2Vec embedding for any given location is thus the patch embedding of the fine-grained cell containing the location. We then evaluate it on predicting downstream socio-economic metrics such as housing prices and population density.

ABSTRACT

Scalable general-purpose representations of the built environment are crucial for geospatial artificial intelligence applications. This paper introduces S2Vec, a novel self-supervised framework for learning such geospatial embeddings. S2Vec uses the S2 Geometry library to partition large areas into discrete S2 cells, rasterizes built environment feature vectors within cells as images, and applies masked autoencoding on these rasterized images to encode the

Permission to make digital or hard copies of all or part of this work for personal or classroom use is granted without fee provided that copies are not made or distributed for profit or commercial advantage and that copies bear this notice and the full citation on the first page. Copyrights for components of this work owned by others than ACM must be honored. Abstracting with credit is permitted. To copy otherwise, or republish, to post on servers or to redistribute to lists, requires prior specific permission and/or a fee. Request permissions from permissions@acm.org.

Conference acronym 'XX, November 03–05, 2025, Minneapolis, MN

© 2025 Association for Computing Machinery.
 ACM ISBN 978-x-xxxx-xxxx-x/YY/MM... \$15.00
<https://doi.org/10.1145/nmmnnnn.nnnnnnn>

feature vectors. This approach yields task-agnostic embeddings that capture local feature characteristics and broader spatial relationships. We evaluate S2Vec on three large-scale socioeconomic prediction tasks, showing its competitive performance against state-of-the-art image-based embeddings. We also explore the benefits of combining S2Vec embeddings with image-based embeddings downstream, showing that such multimodal fusion can often improve performance. Our results highlight how S2Vec can learn effective general-purpose geospatial representations and how it can complement other data modalities in geospatial artificial intelligence.

KEYWORDS

Geospatial AI; Embeddings

ACM Reference Format:

Shushman Choudhury, Elad Aharoni, Chandrakumari Suvarna, Ivel Tsogsuren, Abdul Rahman Kreidieh, Chun-Ta Lu, Neha Arora. 2025. S2Vec:

Self-Supervised Geospatial Embeddings. In *Proceedings of Make sure to enter the correct conference title from your rights confirmation email (Conference acronym 'XX)*. ACM, New York, NY, USA, 10 pages. <https://doi.org/10.1145/nnnnnnn.nnnnnnn>

1 INTRODUCTION

We present a highly scalable and modular approach for developing general-purpose representations of the built environment, i.e., human-made structures and surroundings that enable socioeconomic activity. Such representations, or embeddings, can be adapted through downstream machine learning models for many tasks in geospatial artificial intelligence (or GeoAI) [20, 26]. Socioeconomic applications in urban settings require an understanding of the built environment that is not only fine-grained and precise but also task-agnostic and generalizable across diverse use cases and potentially sparse task-specific datasets [2, 17].

Learning spatial representations and encoding geographic locations is an active area of work within GeoAI, with many recent approaches and even libraries to standardize them [21, 37]. Broadly, these works have focused on the following aspects: encoding a point or a spatial object through analytical functions [22, 23], using aerial and street-level imagery at a location for learning image-based representations [5, 16], and encoding various task-relevant properties at given geographic coordinates [3, 27, 36]. Many of these approaches have proved effective on a range of geospatial classification and regression tasks.

Our key idea (complementary to the above approaches) is twofold: first, we represent a geographic location through built environment features in a grid cell centred at that location; second, we learn embeddings that can capture the feature counts at a location and how they change over a larger area. For the first idea, we use the S2 geometry library [12], an optimized hierarchical geospatial index, to efficiently gather built environment feature vectors at cells of a desired resolution in any large area of interest (e.g., the United States). For the second idea, we rasterize the cell feature vectors as patches in a larger image, and use Masked Autoencoding [14] over the image dataset to learn and generate embeddings for every patch cell in the area of interest. Our approach, which we call S2Vec, is modular and customizable to any area of interest and any desired cell resolution.

We evaluate S2Vec by using its embeddings in a two-layer feed-forward neural network in three downstream socioeconomic regression benchmarks in the GeoAI field: California housing prices, US-wide population density and US-wide median income. As baselines, we use two capable and influential image-based approaches, SATCLIP [16], GEOCLIP [5] and RS-MaMMUT referring to the best performing of the MaMMUT models introduced in [4], to test how embeddings from built environment feature vectors compare with those from imagery. Besides comparing with image embeddings, we also explore various strategies to combine S2Vec with SATCLIP, GEOCLIP and RS-MaMMUT in a multimodal embedding in the downstream model. The built environment is inherently multimodal, and we want to investigate whether and to what extent these two modes can complement each other.

From our experiments, we find that S2Vec alone is competitive with the image embedding baselines on all benchmark tasks. Moreover, using multimodal embeddings typically perform better than

or similar to either of the individual modes. When aggregating signals from multiple embeddings, we find that the choice of fusion strategy between the two modes does not significantly influence performance, though a particular one (project-then-add) is numerically the best fusion strategy across all settings. When we switch the task type to zero-shot geographic adaptation, i.e., where the held-out test set is chosen not at random but as a specific sub-region of the US, we find that S2Vec is typically the best individual mode and that fusing with the best image embedding creates the best overall approach.

In summary, our paper makes the following contributions:

- An efficient and globally scalable scheme for representing locations through features of the built environment using the S2 Geometry geospatial index.
- S2Vec, a framework for learning task-agnostic embeddings of the built environment features, using self-supervised learning through masked autoencoding.
- Large-scale evaluations that compare and combine S2Vec with image-based embeddings on a range of downstream benchmark GeoAI tasks.

The rest of this paper is organized as follows. Section 2 discusses the S2 Geometry library and related work in spatial embeddings, masked autoencoding, and multimodal GeoAI. In Section 3 we describe our S2Vec framework of learning self-supervised geospatial embeddings in detail. Section 4 briefly motivates and discusses our multimodal fusion techniques. We lay out our extensive evaluation setup in Section 5 and reflect on the key themes of the findings in Section 6. Finally, Section 7 concludes with a summary and ideas for future work.

2 BACKGROUND AND RELATED WORK

2.1 S2 Geometry

The S2 Geometry Library, developed by Google, is a comprehensive geospatial computation framework. It partitions the Earth into a hierarchy of cells, known as *S2 cells*, while modeling the Earth as a three-dimensional sphere rather than a flat two-dimensional projection. This design helps preserve spatial locality and enables efficient geometric operations with a single unified coordinate system and geographic database.

Each S2 cell has a unique identifier, allowing for rapid lookups and spatial queries. The hierarchical structure supports multi-resolution analysis and makes it ideal for scalable geospatial applications. In our work, the S2 Geometry Library is fundamental to partitioning a given large geographic area into discrete cells, letting us efficiently extract and arrange built environment features while maintaining the spatial relationships necessary for accurate representation learning.

2.2 Location and Spatial Embeddings

How to represent geographic space effectively in machine learning models is a foundational challenge across GeoAI domains such as remote sensing, urban intelligence, and ecology [25]. A rich body of work has explored this problem [21] and yielded standard benchmarks and frameworks [37]. Three conceptual classes of approaches

are relevant here. First are those that create high-dimensional projections of 2D or 3D coordinates or geometric objects that are learning-friendly, i.e., that task-specific neural networks can use effectively. Example techniques for this encoding approach use multi-frequency sinusoidal functions [22], Fourier transformations [9, 23], double Fourier spheres [27], and spherical harmonics [33].

Second are the approaches that generate embeddings from imagery (either satellite or geo-tagged photographs) using unsupervised or self-supervised contrastive learning techniques, e.g., MO-SAIKS [32], CSP [24], SATCLIP [16] and GEOCLIP [5]. All of these methods have been effectively used in a range of downstream inference tasks. Their specifics and relative strengths vary, but they all benefit from the significant geospatial information contained in images and from powerful techniques in computer vision.

Third, and most relevant for us, are those that use structured attributes from a map, e.g., OpenStreetMaps (OSM) [13] to derive general-purpose representations that capture the semantics of locations. GeoVectors [35] provides a large-scale open corpus of OSM entity embeddings, using neural location embeddings to model spatial relationships and a bag-of-words model on OSM tags for semantics. CityFM [3] updates those ideas using more recent techniques, combining text and visual encoding of tags and geometries respectively. Perhaps the most similar approach to ours at a high level is Hex2vec [36]. It creates vector representations of sets of OSM tags relating to land use and building functions, using Uber’s H3 spatial index (similar to S2 Geometry) to divide a given region into hexagonal cells. The key contrasts with S2Vec are on learning technique and scale; Hex2vec uses the skipgram model with negative sampling to get the embeddings, and is only evaluated on six Polish cities.

2.3 Masked Autoencoding for Representations

Masked autoencoding (MAE) has emerged as a powerful paradigm for self-supervised learning, particularly in visual domains. The pioneering work of He *et al.* [14] showed how deliberately hiding portions of an image at random and training a network to recover the missing content can yield robust and scalable representations. MAE transforms the learning process into a puzzle-solving task by requiring the model to infer the hidden structure from contextual cues.

The Context Autoencoder [7] refines the core MAE idea by emphasizing the role of surrounding information and improving the model’s ability to grasp the underlying semantics of the data. Recognizing that real-world data often spans multiple resolutions, ScaleMAE [30] introduces scale-awareness to capture features at varying levels of detail—a critical capability for applications involving geospatial data. In parallel, the Mixed Autoencoder framework [6] integrates diverse data types into a single reconstruction task, thus enabling more versatile and resilient feature representation. Multimodal Masked Autoencoders [11] jointly learn from different modalities, effectively aligning and transferring knowledge across disparate data sources.

Collectively, these and many other MAE innovations not only enhance our understanding of visual content but also inspire new

approaches for capturing complex, multiscale, and multimodal information. We harness these principles in S2Vec to learn expressive geospatial representations of the built environment.

2.4 Multimodality in Geospatial AI

The built environment is inherently multimodal. To advance Geospatial AI, diverse data modalities have become a driving force, as they allow for rich, multiscale and nuanced representations of urban areas and human activity within them. Broad analyses on foundation models in GeoAI [20, 26, 39, 40] discuss both the promising opportunities and inherent challenges of this integrative approach. For example, combining satellite imagery, street-level views, and other helpful geospatial data can reveal spatial patterns that remain hidden with a single modality [28]. The multimodal fusion enriches the learned representations and includes details that are otherwise overlooked, yielding predictive insights into critical socioeconomic indicators such as income levels, overcrowding, and environmental deprivation [34].

Multimodal data also benefits from creative machine learning techniques. For instance, the SeMAAnD framework [31] uses self-supervised anomaly detection across different geospatial datasets, highlighting the strength of multimodal data in uncovering irregular urban patterns that signal significant changes. Recent research uses heterogeneous graph-based embeddings [41] to model urban regions as interconnected nodes, effectively capturing the complex interplay among various urban elements. Additionally, trajectory-powered models [8, 18] highlight the importance of integrating mobility data with other geospatial signals to create a comprehensive picture of movement within cities.

3 SELF-SUPERVISED GEOSPATIAL EMBEDDINGS

3.1 Problem Definition

We start with a given large geographic landmass of interest \mathcal{A} , e.g., the continental United States of America. We are also given the level l of the S2 cells into which to divide \mathcal{A} , e.g., in all our experiments we use level 12, for which each cell covers a surface area of approximately 5 km².

Let \mathcal{S}_l be the set of all non-overlapping level- l S2 cells that covers the area. Then the ultimate goal of S2Vec is to learn a mapping $\Phi : \mathcal{S}_l \rightarrow \mathbb{R}^n$, where n is the user-specified dimensionality of the embedding. Given any pair of GPS coordinates, S2Vec efficiently looks up the unique level- l S2 cell that contains it, e.g., s_l , and returns $\Phi(s_l)$, the corresponding embedding vector.

S2Vec is designed to be a modular and globally scalable pipeline for encoding properties of geographic locations into fixed-dimensional embeddings. It does so by leveraging efficient hierarchical geospatial indexing and rasterization of built environment feature vectors, and self-supervised representation learning via masked autoencoding (Algorithm 1). The resulting task-agnostic embeddings can then be directly used or aligned with image-based representations in downstream task-specific machine learning models for various geospatial inference applications.

Algorithm 1 How S2Vec learns geospatial embeddings of the built environment**Require:** Geographic Area \mathcal{A} , s2 patch level l , image level $l' < l$, embedding dimensionality n **Ensure:** Embeddings $\phi(s_l)$ for all $s_l \in S_l$ (i.e., all level- l cells covering \mathcal{A})

- 1: Generate and define S2 cells sets $S_l, S_{l'}$ from A
- 2: **for** each $s_l \in S_l$ **do**
- 3: Generate feature vector $\Theta(s_l)$ ▷ Extract built environment features in the cell
- 4: **end for**
- 5: Create rasterized image dataset D , where $D(s_{l'}) = [\Phi(s_{l'}^1), \Phi(s_{l'}^2), \dots]$ and $s_{l'}^i \in \{\text{Children}(s_l)\}$
- 6: Create Masked Auto-Encoding model M with patch encoder dimensionality n
- 7: Train model M on image dataset D ▷ Randomly masked patches are $\Theta(s_l)$ for some $s_l \in S_l$.
- 8: **for** each $s_l \in S_l$ **do**
- 9: Call patch encoding layer of trained M on $\Theta(s_l)$ to get $\phi(s_l)$
- 10: **end for**

3.2 Rasterizing Feature Vector Images

We start with the set of level- l S2 cells (i.e., S_l) into which the large landmass \mathcal{A} has been efficiently partitioned by the S2 Geometry Library. To capture the spatial distribution of built environment features, we represent each S2 cell s_l with a feature vector $\Phi(s_l)$. Specifically, this vector is a histogram of counts that includes:

- **Place-of-Interest Categories:** Counts of various categories of geographic entities within the cell, based on a map’s ontology (e.g., number of shops, restaurants, gas stations, beauty services and so on).
- **Road Network Features:** Counts of infrastructural elements such as roads, traffic lights, and other relevant markers.

Next we need to arrange groups of adjacent s_l cells as patches in images. The set of all such images will be a *disjoint partition* of S_l , i.e., no two images will have any overlapping s_l patches, and the union of all images will use every cell in S_l .

Once again, we leverage the S2 Geometry Library to do this effectively, this time with its hierarchical indexing. We pick a lower level of S2 cells, i.e., $l' < l$, and divide \mathcal{A} into $S_{l'}$, the corresponding set of level- l' cells. By construction, each level- l' comprises exactly $2^{l-l'} \times 2^{l-l'}$ level- l so-called child cells. We map these child s_l cells to their corresponding 2D location within $s_{l'}$ and rasterize the $\Phi(s_l)$ feature vectors (i.e., treating each element as a ‘pixel’ of an image patch unrolled into a 1D vector). As a result, every parent $s_{l'}$ cell now corresponds to a rasterized image of the feature vectors of its child s_l cells, i.e., $D(s_{l'}) = [\Phi(s_l^1), \Phi(s_l^2), \dots]$.

This arrangement of the data preserves spatial continuity and local context of built environment features, while yielding a convenient dataset format on which to apply masked autoencoding, which was designed for images. The data pipeline is agnostic to the feature vector dimensionality, and the patch and image level cells (Section 5 has the specifics for our experiments). It can also leverage distributed processing frameworks to handle global-scale geographic areas.

3.3 Learning Embeddings with MAE

Once we have constructed the rasterized feature vector images, we run masked autoencoding on the image dataset. We follow the original MAE implementation, which is based on the influential Vision Transformer [10]. This self-supervised learning strategy guides

the underlying model to predict missing information based solely on its contextual surroundings. Overall, our MAE yields robust high-quality embeddings that capture (i) the essence of the built environment at a location and (ii) how this property varies spatially over a larger area; both important properties for downstream multi-task geospatial inference.

The following are the broad steps of the MAE in S2Vec (we adapt the language of Section 3 of the original paper [14] where relevant):

- **Random Masking:** Each image has $2^{l-l'} \times 2^{l-l'}$ patches, each corresponding to a feature vector $\Theta(s_l)$ of some child s_l . We sample a subset of patches uniformly at random without replacement and mask (remove) the other ones. The masking of a given image changes each time the image is observed across epochs, which is also a form of data augmentation.
- **Encoding:** This step uses a Vision Transformer on the unmasked patches. The patches are embedded with a standard linear projection and learned positional embeddings and are processed by a set of Transformer blocks. No mask tokens are required as the masked patches are removed. We will also reuse the patch embedding at the end of the process.
- **Decoding:** The decoder is another set of Transformer blocks. It is given both encoded unmasked patches as well as mask tokens (learned vectors that identify which patches are missing and need to be predicted). A key benefit of MAE is the independence of the decoder relative to the encoder, because the former is only used during the self-supervised stage and not for generating the image representations (and in our case, for the patch embeddings). This independence allows it to be typically small and makes the full training much more compute-efficient.
- **Self-Supervision:** The core learning signal comes from a self-supervised reconstruction objective. The model minimizes the difference between the original patches and its reconstructions of the masked ones. This objective guides the network to capture essential spatial patterns and makes it robust to incomplete or noisy inputs. The resulting embeddings will capture both explicit feature counts and implicit spatial correlations, making them highly transferable for many downstream tasks.
- **Generating Patch Embeddings:** After the MAE training is over, we take all s_l cells, lookup their $\Theta(s_l)$ feature vectors,

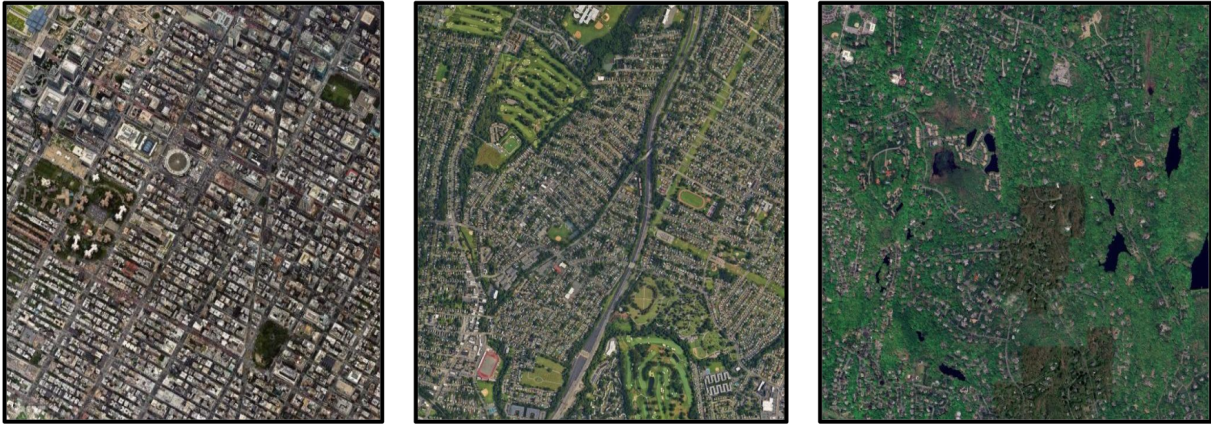


Figure 2: Three distinct kinds of built environment areas that help illustrate how S2Vec and image-based representations could complement each other. The left (downtown) and middle (suburb) would have some overlap in feature vector space, as would the middle and right (rural). But overhead imagery could help distinguish different kinds of suburbs (for instance) depending on the spatial arrangement of the built environment features. The images are taken from Google Maps’ satellite view.

and run the trained patch encoder on each $\Theta(s_i)$ to get the corresponding $\Phi(s_i)$ embedding. In contrast, the original MAE model, when used on image recognition, encodes the entire image to get its latent representation. We do not care about image-level (l') representations, only patch-level (l) ones. But if a downstream application would benefit from embeddings for coarser-grained image-level cells, i.e., $\Phi(s_{l'})$, then S2Vec would be suitable for those as well.

4 FUSING WITH IMAGE EMBEDDINGS

The data modality captured in S2Vec is essentially a geospatial knowledge database, which is used to generate the feature vectors of counts for each S2 cell. This is one of several modalities that are useful and relevant for GeoAI applications; others include plain text, street view and remote sensing images, mobility data, and vector representations ([20]; Section 4). Of these other modes, imagery in particular has the potential to align with and complement S2Vec (illustrated in Figure 2).

To empirically assess the benefits of such multimodal representations, we explore fusing the S2Vec embeddings with separately trained image-based embeddings in the downstream task-specific models (we use three different image-based embeddings as mentioned in Section 5.3). We try three different commonly-used strategies for the two sets of embeddings:

- (1) **Concatenation:** We concatenate the embedding vectors to form a joint representation whose length is the sum of the two embedding dimensionalities.
- (2) **Weighted Addition:** We apply learnable weights to each embedding before element-wise addition; this only works if the two sets of embeddings have the same dimensionality.
- (3) **Projection and Addition:** We separately project each embedding with a hidden layer to the same dimensionality and then add them element-wise.

These techniques will allow us to examine how different fusion methods impact performance on downstream tasks, and whether

and to what extent the built environment and image-based representations can complement each other.

5 EVALUATION

5.1 S2Vec Implementation Details

In our experiments, we select the level of an image S2 cell to be 8 and that of a patch cell to be 12, which ultimately leads to $2^{12-8} \times 2^{12-8} = 16 \times 16 = 256$ patch level cells per image cell. A single level 8 S2 cell covers an area of approximately 1300 km^2 , and a level 12 S2 cell covers an area of approximately 5 km^2 .

We implement a distributed parallel processing pipeline to generate the feature vectors and images. This pipeline begins by querying Google Maps Road Network data (e.g., lanes, Points Of Interest) to retrieve the environment features for each patch level S2 cell. For each patch level cell, identified by its unique key, we construct a histogram feature vector of size 116. The first 115 indices of this vector represent the counts of place-of-interest categories, while the last index is the total number of roads within that patch level S2 cell. To enable normalization in subsequent steps, we also compute the column-wise mean and variance across all the generated patch level feature vectors.

Subsequently, we use the S2 Geometry Library to rasterize the chosen image level S2 cells. This rasterization involves ordering the patch level cells within each image level cell row by row, starting from the top-left corner and proceeding to the bottom-right. To obtain the final unrolled feature vector for an image cell, we concatenate the individual histogram feature vectors of all the ordered patch cells into a single vector. Using this pipeline, we generate an image dataset for the entire US, comprising around 12000 images. Our globally scalable pipeline uses Apache Beam with both C++ for the raw features and Python for the rasterization.

Pre-training Details: Prior to pre-training, we globally normalize all feature vectors with feature-wise means and variances. S2Vec uses the core masked autoencoding architecture from the original paper, but with specific hyperparameter settings tailored

Table 1: S2Vec Pre-Training Hyper-parameters

Hyperparameter	Value
MAE Architecture	
Attention Heads	8
Encoder Layers	6
Decoder Layers	2
Encoder Dimension	256
Decoder Dimension	128
Optimizer	
Name	AdamW
Weight Decay	0.001
Clipnorm	1.0
Initial Learning Rate	5e-4
Alpha (α)	0.1
Training	
Batch Size	64
Shuffle Buffer Size	1000
Number of Epochs	50
Dropout Rate	0.2

for our task. We use the AdamW optimizer [19] along with a cosine decay learning rate schedule. Table 1 summarizes the specific pre-training hyperparameters we used. We tune these hyperparameters through an extensive black box random sampling process, using the pre-training loss on a randomly held-out validation set to pick the best set.

Across all our experiments, the embedding dimensionality is consistently set to 256. We use Tensorflow 2.0 and Keras with Python for all the model code. The pre-training hyperparameter tuning and final runs are all done on 8 Nvidia V100 GPUs, with distributed training using Tensorflow’s mirrored data parallelism strategy [1].

5.2 Downstream Tasks and Models

To test how well the S2Vec embeddings work in different situations, we ran experiments on three predictive modeling tasks over diverse and representative geographic regions: California housing prices [29], US-wide population density [32], and US-wide median income [15]. These datasets differ in geographic resolution—while the first two provide values at specific coordinates, the third aggregates data at the ZIP code level.

To ensure consistency across datasets, we lined up all data points to level 12 S2 cells. This gave us approximately 6700 data points for the California housing prices dataset, 47000 data points for US-wide population density, and 1.7 million data points for US median income. In cases where multiple data points fall within the same S2 cell, we assign the median label for that cell.

For downstream predictive modeling, we use a two-layer multi-layer perceptron on top of the learned S2Vec embeddings to predict the regression targets. Before training, we scaled all the target values (like prices and income) to be between 0 and 1; this is a common trick to help the model learn better and more easily. Each



Figure 3: The eastern portion of the US that we hold-out in geographic adaptation experiments. This area is used as the final test set to evaluate the downstream models after training and validation on the remaining area.

downstream model was trained using the mean squared error loss function and AdamW as the optimizer.

We tuned the downstream model hyperparameters by sweeping over a predefined set of values for the learning rate, number of hidden units, and dropout rate on an independent validation set. We then use the best-performing set of hyperparameters to train the model on the training set, with early stopping based on the validation set loss to prevent overfitting. Finally, we evaluate the model on the held-out test set. This entire end-to-end process is repeated with multiple random seeds for more robust results. The scheme described here is standard for evaluating general-purpose embeddings and is very similar to the specific steps used in SATCLIP [16]. The downstream experiments are conducted with a Python Colab notebook on a single V100 GPU.

5.3 Methods Compared

Our experiments compare several different methods and variations; we discuss them here in stages.

Unimodal Embeddings: First, we compare S2Vec individually with other image-based embeddings:

- **SATCLIP:** A contrastive vision-language model tailored for remote sensing, aligning satellite imagery with textual descriptions. [16]. We use the ResNet18 backbone with L=40 legendre polynomials; the embeddings are 256 in length.
- **GEOCLIP:** A CLIP-inspired geo-localization model that aligns remote-sensing imagery with encoded location. [5]. We use the default open source setting that produces embeddings that are 512 in length.
- **RS-MaMUT:** A pre-trained RGB remote sensing vision-language model based on the MaMUT architecture. [4]. The embeddings are 1152 in length.

Adding Location Signal: Neither S2Vec nor RS-MaMUT use the location (i.e., the numerical coordinates or some derived form of them) of the S2 cells or the image in their pre-training. SATCLIP and GEOCLIP, however, explicitly encode the coordinates of the images in pre-training. Socioeconomic metrics can vary considerably based only on location, e.g., the median income in a zipcode in one US state may be very different from a zipcode in another even if their overhead imagery and built environment features are similar. Thus,

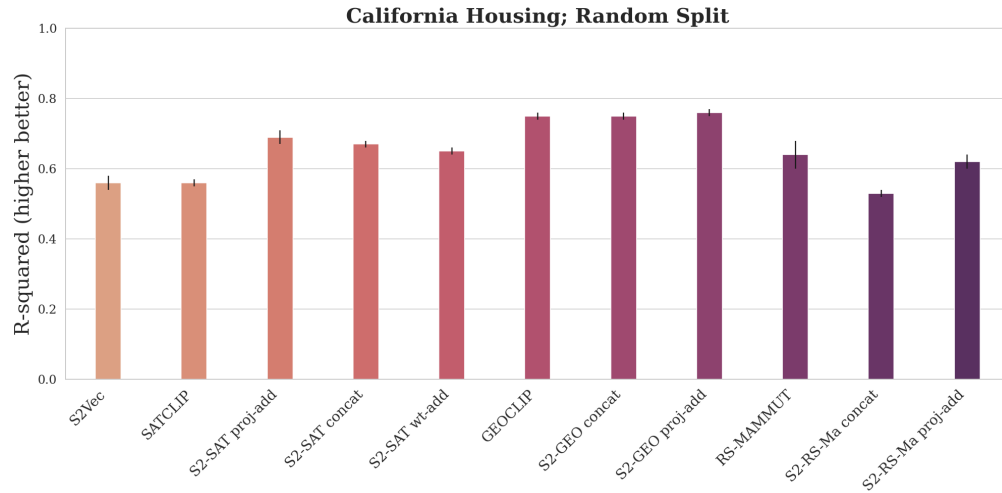


Figure 4: On the California house price task, for individual modes S2Vec is comparable with SATCLIP, but RS-MaMAMMUT is better and GEOCLIP is the best. Fusing S2Vec with SATCLIP/GEOCLIP outperforms either mode, except with RS-MaMAMMUT where the fusion is likely overfitting on the relatively small dataset.

to enable a fairer comparison with SATCLIP and GEOCLIP on the two US-wide tasks, and more broadly to evaluate to what extent the location signal helps S2Vec and RS-MaMAMMUT we have variants that include a location encoding (named S2Vec-Loc and so on).

To include a location signal, we generate the Space2Vec analytical encoding [22] for the centroid of the s2 cell of each datapoint and concatenate it with the respective embeddings in the downstream model. This encoding is just one simple way to add the location signal, and exploring this further or optimizing it for a downstream task is out of the scope of this work.

Multimodal Fusion: Finally, we combine S2Vec with each image-based embedding in turn to evaluate the multimodal fusion; they are named S2-SATC, S2-GEOC, and S2-RS-Ma for conciseness. As discussed in Section 4, we try up to three different strategies (named concat, wt-add, and proj-add for conciseness). The wt-add variant, i.e., addition with learnable weights, only works for S2-SATC as they have the same length. For S2-RS-Ma, we also have a variant with the location signal included.

As with the task datasets, we made sure everything was lined up with level 12 S2 cells. The SATCLIP and GEOCLIP models give us embeddings for specific points. We generated embeddings that matched the locations in our datasets and used those in our prediction tasks. If an S2 cell had multiple geographic coordinates, we used the average of their embeddings. For RS-MaMAMMUT embedding generation, we process 1020x1020 pixel image crops centered on each level 12 S2 cell. These patches, representing a 2m/pixel ground resolution, are extracted from high-resolution satellite imagery between March 2021 and March 2025.

5.4 Results

We use a similar downstream evaluation scheme as SATCLIP [16]. For a given dataset and a given embedding method, we define the downstream model using the embedding and the best set of hyperparameters for that method (as described in Section 5.2). Then,

over 20 random train/validation/test splits of the dataset (using a 60/20/20 split), we train the downstream model on the training set, use early stopping based on the validation set, and evaluate on the held-out test set.

For the 2 US datasets, we run an additional set of experiments on so-called *zero-shot geographic adaptation*, or how well the embeddings generalize across space. Here the train/validation/test split is not random but spatial, i.e., we hold out an entire sub-geography and use the remaining area for training and validation. For our experiments, we holdout the northern and eastern parts of the USA as shown in Figure 3. For this task type, since we use the location coordinates to split the data, we do not evaluate the variants of S2Vec or RS-MaMAMMUT with the location encoding.

We report two evaluation metrics on the held-out test set: the R^2 metric and the Mean Absolute Error metric. The R^2 metric (typically between 0 and 1; higher is better) is a goodness-of-fit metric that measures how well the regression predictions approximate the real data points. The Mean Absolute Error (Mean. Abs. Err; lower better) is a ubiquitous error metric in machine learning; here we report the Mean Abs. Err. for the normalized regression target (between 0 and 1) to make it more interpretable. Both metrics are informative and useful; we vary which one we report across experiments.

5.4.1 Random Train/Val/Test Split. The bar plot in Figure 4 shows how the various approaches compare in terms of the R^2 metric on the California housing price task. Among the unimodal embeddings, GEOCLIP performs the best, which is consistent with the benchmarking from the earlier SATCLIP paper ([16]; Table 2). Then comes RS-MaMAMMUT, and then close behind are S2Vec and SATCLIP, both of which are comparable to each other.

Generally, methods combining S2Vec with other modalities (S2-SAT, S2-GEO) tend to outperform either of the individual modes. The exception to this is with RS-MaMAMMUT, where the multimodal alignment hurts performance. However, this is most likely due to

Table 2: Random train/validation/test split performance on the two US-wide datasets: population and median income. Over 20 independently initialized training runs, we report the mean and standard deviation of the Mean Absolute Error (lower better) over the min-max scaled held-out test set.

Method	Population Mean Abs. Err. ↓	Median Income Mean Abs. Err. ↓
<i>Unimodal</i>		
S2Vec	0.065 ± 0.002	0.057 ± 5e-5
SATCLIP	0.075 ± 0.001	0.044 ± 1e-3
GEOCLIP	0.075 ± 0.005	0.033 ± 6e-5
RS-MaMMUT	0.057 ± 4e-4	0.061 ± 2e-3
<i>With Location</i>		
S2Vec-Loc	0.065 ± 3e-4	0.054 ± 5e-5
RS-MaMMUT-Loc	0.057 ± 3e-4	0.058 ± 2e-3
<i>Multimodal</i>		
S2-SATC proj-add	0.065 ± 0.003	0.045 ± 2e-3
S2-GEOC proj-add	0.066 ± 0.003	0.045 ± 3e-3
S2-RS-Ma proj-add	0.058 ± 4e-4	0.056 ± 2e-4
S2-RS-Ma proj-add-Loc	0.057 ± 3e-4	0.055 ± 1e-4

overfitting on the relatively small dataset of 6600 datapoints and the higher embedding dimensionality of 1152 for RS-MaMMUT (compared with 256 for S2Vec/SATCLIP and 512 for GEOCLIP). Finally, the project-add approach (proj-add) is the best for multimodal alignment regardless of which two methods are used. This relative superiority of proj-add was repeated for the remaining tasks; for better readability, **subsequent results will only report proj-add among the fusion approaches.**

Next, Table 2 reports Mean Absolute Error of the various methods on the two larger and more robust US-wide tasks, Population and Median Income. For each column, the method with the lowest Mean Abs. Err. is boldfaced. On the Population task, RS-MaMMUT alone outperforms all other approaches, including the multimodal fusions, while S2Vec is second on individual modes. For each of SATCLIP and GEOCLIP, fusing with S2Vec through project-add improves on both of them individually (though not on S2Vec alone), while fusing S2Vec with RS-MaMMUT improves on the former but not the latter. Adding location signal for this task does not appear to improve any of the approaches to which it is added.

On median income, however, GEOCLIP performs the best overall. Fusing S2Vec with SATCLIP, GEOCLIP, and RS-MaMMUT improves on S2Vec in all cases and on RS-MaMMUT, though not on SATCLIP or GEOCLIP. Unlike in the previous dataset, adding the location signal here improves on all three approaches to which it is added. This difference supports the intuition that the median income task depends strongly on the underlying geographic location regardless of the built environment or the overhead imagery. This location dependence also helps explain the relatively strong performance of GEOCLIP and SATCLIP, which encode location explicitly during pre-training (rather than just combining them downstream in a lightweight manner).

Table 3: Zero-shot Geographic Adaptation performance on the two US-wide datasets: population and median income. Over 20 independently initialized training runs, we report the mean and standard deviation of the R^2 metric (higher better) over the held-out test set.

Method	Population R^2 ↑	Median Income R^2 ↑
<i>Unimodal</i>		
S2Vec	0.64 ± 0.004	0.45 ± 0.006
SATCLIP	-0.6 ± 0.35	-7.24 ± 0.87
GEOCLIP	0.33 ± 0.01	0.30 ± 0.02
RS-MaMMUT	0.68 ± 0.008	0.23 ± 0.03
<i>Multimodal</i>		
S2-SATC proj-add	0.56 ± 0.01	0.37 ± 0.01
S2-GEOC proj-add	0.6 ± 0.01	0.48 ± 0.01
S2-RS-Ma proj-add	0.72 ± 0.006	0.35 ± 0.007

5.4.2 Zero-Shot Geographic Adaptation. Table 3 reports the R^2 metric for all approaches on the zero-shot adaptation task, where the held-out test set is from the eastern part of the US and entirely removed from the training and validation sets. Here, we find that S2Vec significantly outperforms both SATCLIP and GEOCLIP individually on both datasets. Between RS-MaMMUT and S2Vec, the former is the best individual mode on the population dataset and the latter is the best individual mode on the median income dataset.

The effect of multimodal fusion in this task type is more pronounced than in the random split task. On the population dataset, the multimodal embedding improves on the image-based embedding in all cases, but only improves on S2Vec in the S2-RS-Ma case; S2-RS-Ma is the best overall. On the median income dataset, where S2Vec is significantly better than all other approaches, only S2-GEOCLIP (the overall winner) improves on it. Again, for all image-based embeddings in this dataset, fusing with S2Vec improves against the image-only metric.

6 DISCUSSION

Our work highlights several key insights regarding geospatial representation learning. First, S2Vec works much better in the geographic adaptation task than in the random split task. Zero-shot geographic adaptation, where the model is tested on a completely unseen region, is in some ways more difficult and arguably more important for making models that can work anywhere in the world – a key goal for geospatial foundation models. The strong performance of S2Vec here shows the value of encoding built environment features in a way that captures spatial relationships and depends less on specific regional patterns learned from training data.

Second, the results from our multimodal fusion experiments present a mixed but useful signal. Usually, combining S2Vec with image data improves the results compared to using either one alone, suggesting that they effectively complement each other. However, this improvement doesn't happen when one of the individual methods is already very good or the best at a task. Also, note that in

our experiments, the embeddings are fused after independent pre-training. Such downstream fusion may limit how much they help each other compared to combining them during pre-training.

Third, S2Vec uses a lightweight approach by leveraging built environment feature vectors and masked autoencoding. Despite being relatively simple in comparison to the image-based models, S2Vec achieves competitive performance across various socioeconomic prediction tasks. This effectiveness is at least in part due to the hierarchical multi-resolution aspect of the S2 Geometry Library, which allows for efficient partitioning of large geographic areas into cells of varying resolutions. This hierarchical structure enables S2Vec to capture both fine-grained local features and broader spatial relationships by rasterizing feature vectors from fine-grained cells into images of coarser-grained cells.

Overall, S2Vec and our results are important for how we learn to represent geospatial data and build foundation models. S2Vec offers a scalable and versatile approach to encode built environment information, yielding strong performance across various socioeconomic prediction tasks. We also show how it is useful to combine different types of data and different encoding techniques to capture the complexity of geospatial data. As we work towards more general and powerful geospatial foundation models, methods like S2Vec give us valuable tools and ideas for representing and understanding the world around us.

7 CONCLUSION

In this paper, we introduced S2Vec, a scalable self-supervised framework for learning geospatial embeddings of the built environment. S2Vec uses the S2 Geometry Library for efficient spatial partitioning, rasterizes built environment feature vectors, and learns powerful and task-agnostic representations with masked autoencoding. Our evaluations on downstream socioeconomic prediction tasks demonstrate that S2Vec is competitive with image-based embedding methods and that multimodal fusion with image-based embeddings often leads to improved performance, highlighting the complementary nature of different geospatial data modalities.

Our work lays a foundation for several promising avenues of future research. First, we could use significantly richer feature vectors to represent a cell and location. Beyond counts of built environment features, future work could explore encoding other valuable geospatial information, such as overhead building geometries, elevation profiles, and time-dependent features related to mobility patterns and traffic flow. Having such diverse data sources would lead to even more comprehensive and informative embeddings. Second, while this work uses the masked autoencoding approach inspired by the Vision Transformer, other architectures could be explored that better leverage structured geospatial relationships. For example, graph transformer networks [38] could explicitly model the complex relationships and dependencies between neighboring cells or other geospatial entities.

Third, the core S2Vec framework could be adapted to learn spatially aware embeddings of other geospatial entities beyond grid cells, such as points of interest, road networks, and other vector-based geographic data. Developing methods to effectively represent and relate these different types of geospatial information is a critical challenge in GeoAI. Finally, an important direction for future work

could be joint pre-training strategies. Instead of fusing embeddings from independently pre-trained models, future research could explore joint pre-training with overhead imagery and feature vectors through multi-channel masked autoencoding. This would allow the model to learn cross-modal representations in a more integrated manner, potentially leading to even more powerful embeddings.

ACKNOWLEDGMENTS

The authors would like to thank Pranjal Awasthi, Nadav Sherman, Genady Beryozkin, and Tomer Shekel (all from Google Research) for valuable comments and insights.

REFERENCES

- [1] Martin Abadi, Ashish Agarwal, Paul Barham, Eugene Brevdo, Zhifeng Chen, Craig Citro, Greg S Corrado, Andy Davis, Jeffrey Dean, Matthieu Devin, et al. 2016. Tensorflow: Large-scale machine learning on heterogeneous distributed systems. *arXiv preprint arXiv:1603.04467* (2016).
- [2] Mohit Agarwal, Mimi Sun, Chaitanya Kamath, Arbaaz Muslim, Prithul Sarker, Joydeep Paul, Hector Yee, Marcin Sieniek, Kim Jablonski, Yael Mayer, et al. 2024. General Geospatial Inference with a Population Dynamics Foundation Model. *arXiv preprint arXiv:2411.07207* (2024).
- [3] Pasquale Balsebre, Weiming Huang, Gao Cong, and Yi Li. 2023. City Foundation Models for Learning General Purpose Representations from OpenStreetMap. *arXiv preprint arXiv:2310.00583* (2023).
- [4] Aviad Barzilai, Yotam Gigi, Amr Helmy, Vered Silverman, Yehonathan Refael, Bolous Jaber, Tomer Shekel, George Leifman, and Genady Beryozkin. 2025. A Recipe for Improving Remote Sensing VLM Zero Shot Generalization. *arXiv:2503.08722* [cs.CV] <https://arxiv.org/abs/2503.08722>
- [5] Vicente Vivanco Cepeda, Gaurav Kumar Nayak, and Mubarak Shah. 2023. GeoCLIP: Clip-Inspired Alignment between Locations and Images for Effective Worldwide Geo-localization. In *Advances in Neural Information Processing Systems 36: Annual Conference on Neural Information Processing Systems 2023, NeurIPS 2023, New Orleans, LA, USA, December 10 - 16, 2023*, Alice Oh, Tristan Naumann, Amir Globerson, Kate Saenko, Moritz Hardt, and Sergey Levine (Eds.). http://papers.nips.cc/paper_files/paper/2023/hash/1b57aaddf85ab01a2445a79c9edc1f4b-Abstract-Conference.html
- [6] Kai Chen, Zhili Liu, Lanqing Hong, Hang Xu, Zhenguo Li, and Dit-Yan Yeung. 2023. Mixed Autoencoder for Self-Supervised Visual Representation Learning. In *IEEE/CVF Conference on Computer Vision and Pattern Recognition, CVPR 2023, Vancouver, BC, Canada, June 17-24, 2023*. IEEE, 22742–22751. <https://doi.org/10.1109/CVPR52729.2023.02178>
- [7] Xiaokang Chen, Mingyu Ding, Xiaodi Wang, Ying Xin, Shentong Mo, Yunhao Wang, Shumin Han, Ping Luo, Gang Zeng, and Jingdong Wang. 2024. Context Autoencoder for Self-supervised Representation Learning. *Int. J. Comput. Vis.* 132, 1 (2024), 208–223. <https://doi.org/10.1007/S11263-023-01852-4>
- [8] Shushman Choudhury, Abdul Rahman Kreidieh, Ivan Kuznetsov, and Neha Arora. 2024. Towards a Trajectory-powered Foundation Model of Mobility. In *Proceedings of the 3rd ACM SIGSPATIAL International Workshop on Spatial Big Data and AI for Industrial Applications, GeoIndustry 2024, Atlanta, GA, USA, 29 October 2024 - 1 November 2024*, Jimeng Rao, Emre Eftelioglu, Heba Aly, Yiqun Xie, and Song Gao (Eds.). ACM, 1–4. <https://doi.org/10.1145/3681766.3699610>
- [9] Maria Despoina Siampou, Jialiang Li, John Krumm, Cyrus Shahabi, and Hua Lu. 2024. Poly2Vec: Polymorphic Encoding of Geospatial Objects for Spatial Reasoning with Deep Neural Networks. *arXiv e-prints* (2024), arXiv–2408.
- [10] Alexey Dosovitskiy, Lucas Beyer, Alexander Kolesnikov, Dirk Weissenborn, Xiao-hua Zhai, Thomas Unterthiner, Mostafa Dehghani, Matthias Minderer, G Heigold, S Gelly, et al. 2020. An Image is Worth 16x16 Words: Transformers for Image Recognition at Scale. In *International Conference on Learning Representations*.
- [11] Xinyang Geng, Hao Liu, Lisa Lee, Dale Schuurmans, Sergey Levine, and Pieter Abbeel. 2022. Multimodal masked autoencoders learn transferable representations. *arXiv preprint arXiv:2205.14204* (2022).
- [12] Google. [n. d.]. The S2 Geomet library. <http://s2geometry.io/>
- [13] Mordechai Haklay and Patrick Weber. 2008. Openstreetmap: User-generated street maps. *IEEE Pervasive computing* 7, 4 (2008), 12–18.
- [14] Kaiming He, Xinlei Chen, Saining Xie, Yanghao Li, Piotr Dollár, and Ross Girshick. 2022. Masked Autoencoders Are Scalable Vision Learners. In *2022 IEEE/CVF Conference on Computer Vision and Pattern Recognition (CVPR)*. IEEE, 15979–15988.
- [15] Junting Jia and Auston R Benson. 2020. Residual correlation in graph neural network regression. In *Proceedings of the 26th ACM SIGKDD international conference on knowledge discovery & data mining*. 588–598.
- [16] Konstantin Klemmer, Esther Rolf, Caleb Robinson, Lester Mackey, and Marc Rußwurm. 2023. Satclip: Global, general-purpose location embeddings with

- satellite imagery. *arXiv preprint arXiv:2311.17179* (2023).
- [17] Alexandre Lacoste, Nils Lehmann, Pau Rodríguez, Evan D. Sherwin, Hannah Kerner, Björn Lütjens, Jeremy Irvin, David Dao, Hamed Alemohammad, Alexandre Drouin, Mehmet Gunturkun, Gabriel Huang, David Vázquez, Dava Newman, Yoshua Bengio, Stefano Ermon, and Xiaoxiang Zhu. 2023. GEO-Bench: Toward Foundation Models for Earth Monitoring. In *Advances in Neural Information Processing Systems 36: Annual Conference on Neural Information Processing Systems 2023, NeurIPS 2023, New Orleans, LA, USA, December 10 - 16, 2023*, Alice Oh, Tristan Naumann, Amir Globerson, Kate Saenko, Moritz Hardt, and Sergey Levine (Eds.). http://papers.nips.cc/paper_files/paper/2023/hash/a0644215d9cff6646fa334dfa5d29c5a-Abstract-Datasets_and_Benchmarks.html
- [18] Yan Lin, Tonglong Wei, Zeyu Zhou, Haomin Wen, Jilin Hu, Shengnan Guo, Youfang Lin, and Huaiyu Wan. 2024. TrajFM: A Vehicle Trajectory Foundation Model for Region and Task Transferability. *arXiv preprint arXiv:2408.15251* (2024).
- [19] Ilya Loshchilov and Frank Hutter. 2017. Decoupled weight decay regularization. *arXiv preprint arXiv:1711.05101* (2017).
- [20] Gengchen Mai, Weiming Huang, Jin Sun, Suhang Song, Deepak Mishra, Ninghao Liu, Song Gao, Tianming Liu, Gao Cong, Yingjie Hu, Chris Cundy, Ziyuan Li, Rui Zhu, and Ni Lao. 2024. On the Opportunities and Challenges of Foundation Models for GeoAI (Vision Paper). *ACM Trans. Spatial Algorithms Syst.* 10, 2 (2024), 11. <https://doi.org/10.1145/3653070>
- [21] Gengchen Mai, Krzysztof Janowicz, Yingjie Hu, Song Gao, Bo Yan, Rui Zhu, Ling Cai, and Ni Lao. 2022. A review of location encoding for GeoAI: methods and applications. *International Journal of Geographical Information Science* 36, 4 (2022), 639–673.
- [22] Gengchen Mai, Krzysztof Janowicz, Bo Yan, Rui Zhu, Ling Cai, and Ni Lao. 2020. Multi-Scale Representation Learning for Spatial Feature Distributions using Grid Cells. In *8th International Conference on Learning Representations, ICLR 2020, Addis Ababa, Ethiopia, April 26-30, 2020*. OpenReview.net. <https://openreview.net/forum?id=JlJldh4KDH>
- [23] Gengchen Mai, Chiyu Jiang, Weiwei Sun, Rui Zhu, Yao Xuan, Ling Cai, Krzysztof Janowicz, Stefano Ermon, and Ni Lao. 2023. Towards general-purpose representation learning of polygonal geometries. *Geoinformatica* 27, 2 (2023), 289–340.
- [24] Gengchen Mai, Ni Lao, Yutong He, Jiaming Song, and Stefano Ermon. 2023. CSP: Self-Supervised Contrastive Spatial Pre-Training for Geospatial-Visual Representations. In *International Conference on Machine Learning, ICML 2023, 23-29 July 2023, Honolulu, Hawaii, USA (Proceedings of Machine Learning Research, Vol. 202)*, Andreas Krause, Emma Brunskill, Kyunghyun Cho, Barbara Engelhardt, Sivan Sabato, and Jonathan Scarlett (Eds.). PMLR, 23498–23515. <https://proceedings.mlr.press/v202/mai23a.html>
- [25] Gengchen Mai, Ziyuan Li, and Ni Lao. [n. d.]. Spatial Representation Learning in GeoAI. In *Handbook of Geospatial Artificial Intelligence*. CRC Press, 99–120.
- [26] Gengchen Mai, Yiqun Xie, Xiaowei Jia, Ni Lao, Jinneng Rao, Qing Zhu, Zeping Liu, Yao-Yi Chiang, and Junfeng Jiao. 2025. Towards the next generation of Geospatial Artificial Intelligence. *International Journal of Applied Earth Observation and Geoinformation* 136 (2025), 104368.
- [27] Gengchen Mai, Yao Xuan, Wenyun Zuo, Yutong He, Jiaming Song, Stefano Ermon, Krzysztof Janowicz, and Ni Lao. 2023. Sphere2Vec: A general-purpose location representation learning over a spherical surface for large-scale geospatial predictions. *ISPRS Journal of Photogrammetry and Remote Sensing* 202 (2023), 439–462.
- [28] Vishal Nedungadi, Ankit Karirya, Stefan Oehmcke, Serge J. Belongie, Christian Igel, and Nico Lang. 2024. MMEarth: Exploring Multi-modal Pretext Tasks for Geospatial Representation Learning. In *Computer Vision - ECCV 2024 - 18th European Conference, Milan, Italy, September 29-October 4, 2024, Proceedings, Part LXIV (Lecture Notes in Computer Science, Vol. 15122)*, Ales Leonardis, Elisa Ricci, Stefan Roth, Olga Russakovsky, Torsten Sattler, and Gül Varol (Eds.). Springer, 164–182. https://doi.org/10.1007/978-3-031-73039-9_10
- [29] R Kelley Pace and Ronald Barry. 1997. Sparse spatial autoregressions. *Statistics & Probability Letters* 33, 3 (1997), 291–297.
- [30] Colorado J. Reed, Ritwik Gupta, Shufan Li, Sarah Brockman, Christopher Funk, Brian Clipp, Kurt Keutzer, Salvatore Candido, Matt Uyttendaele, and Trevor Darrell. 2023. Scale-MAE: A Scale-Aware Masked Autoencoder for Multiscale Geospatial Representation Learning. In *IEEE/CVF International Conference on Computer Vision, ICCV 2023, Paris, France, October 1-6, 2023*. IEEE, 4065–4076. <https://doi.org/10.1109/ICCV51070.2023.00378>
- [31] Daria Reshetova, Swetava Ganguli, C. V. Krishnakumar Iyer, and Vipul Pandey. 2023. SeMAnD: Self-Supervised Anomaly Detection in Multimodal Geospatial Datasets. In *Proceedings of the 31st ACM International Conference on Advances in Geographic Information Systems, SIGSPATIAL 2023, Hamburg, Germany, November 13-16, 2023*, Matthias Renz and Mario A. Nascimento (Eds.). ACM, 61:1–61:4. <https://doi.org/10.1145/3589132.3625604>
- [32] Esther Rolf, Jonathan Proctor, Tamma Carleton, Ian Bolliger, Vaishaal Shankar, Miyabi Ishihara, Benjamin Recht, and Solomon Hsiang. 2021. A generalizable and accessible approach to machine learning with global satellite imagery. *Nature communications* 12, 1 (2021), 4392.
- [33] Marc Rußwurm, Konstantin Klemmer, Esther Rolf, Robin Zbinden, and Devis Tuia. 2023. Geographic location encoding with spherical harmonics and sinusoidal representation networks. *arXiv preprint arXiv:2310.06743* (2023).
- [34] Esra Suel, Samir Bhatt, Michael Brauer, Seth Flaxman, and Majid Ezzati. 2021. Multimodal deep learning from satellite and street-level imagery for measuring income, overcrowding, and environmental deprivation in urban areas. *Remote Sensing of Environment* 257 (2021), 112339.
- [35] Nicolas Tempelmeier, Simon Gottschalk, and Elena Demidova. 2021. GeoVectors: A Linked Open Corpus of OpenStreetMap Embeddings on World Scale. In *CIKM '21: The 30th ACM International Conference on Information and Knowledge Management, Virtual Event, Queensland, Australia, November 1 - 5, 2021*, Gianluca Demartini, Guido Zuccon, J. Shane Culpepper, Zi Huang, and Hanghang Tong (Eds.). ACM, 4604–4612. <https://doi.org/10.1145/3459637.3482004>
- [36] Szymon Wozniak and Piotr Szymanski. 2021. hex2vec: Context-Aware Embedding H3 Hexagons with OpenStreetMap Tags. In *GeoAI@SIGSPATIAL 2021: Proceedings of the 4th ACM SIGSPATIAL International Workshop on AI for Geographic Knowledge Discovery, Beijing, China, November 2, 2021*, Dalton D. Lunga, Hsiuhan Lexie Yang, Song Gao, Bruno Martins, Yingjie Hu, Xueqing Deng, and Shawn D. Newsam (Eds.). ACM, 61–71. <https://doi.org/10.1145/3486635.3491076>
- [37] Nemin Wu, Qian Cao, Zhangyu Wang, Zeping Liu, Yanlin Qi, Jieli Zhang, Joshua Ni, X Angela Yao, Hongxu Ma, Lan Mu, et al. 2024. TorchSpatial: A Location Encoding Framework and Benchmark for Spatial Representation Learning. In *The Thirty-eight Conference on Neural Information Processing Systems Datasets and Benchmarks Track*.
- [38] Seongjun Yun, Minbyul Jeong, Raehyun Kim, Jaewoo Kang, and Hyunwoo J Kim. 2019. Graph transformer networks. *Advances in neural information processing systems* 32 (2019).
- [39] Weijia Zhang, Jindong Han, Zhao Xu, Hang Ni, Hao Liu, and Hui Xiong. 2024. Towards Urban General Intelligence: A Review and Outlook of Urban Foundation Models. *arXiv preprint arXiv:2402.01749* (2024).
- [40] Yue Zhou, Litong Feng, Yiping Ke, Xue Jiang, Junchi Yan, Xue Yang, and Wayne Zhang. 2024. Towards Vision-Language Geo-Foundation Model: A Survey. *arXiv preprint arXiv:2406.09385* (2024).
- [41] Xingchen Zou, Jiani Huang, Xixuan Hao, Yuhao Yang, Haomin Wen, Yibo Yan, Chao Huang, Chao Chen, and Yuxuan Liang. 2025. Space-aware Socioeconomic Indicator Inference with Heterogeneous Graphs. *arXiv:2405.14135 [cs.LG]* <https://arxiv.org/abs/2405.14135>